

# Subunit Dependencies of *N*-Methyl-D-aspartate (NMDA) Receptor-Induced $\alpha$ -Amino-3-hydroxy-5-methyl-4-isoxazolepropionic Acid (AMPA) Receptor Internalization<sup>§</sup>

C. M. Tigaret, A. Thalhammer, G. F. Rast, C. G. Specht,<sup>1</sup> Y. P. Auberson, M. G. Stewart, and R. Schoepfer

Laboratory for Molecular Pharmacology, Department of Pharmacology, University College London, London, United Kingdom (C.M.T., A.T., G.F.R., C.G.S., R.S.); Novartis Institutes for Biomedical Research, Novartis Pharma AG, Basel, Switzerland (Y.P.A.); and Department of Biological Sciences, The Open University, Milton Keynes, United Kingdom (M.G.S.)

Received September 6, 2005; accepted January 24, 2006

## ABSTRACT

*N*-Methyl-D-aspartate (NMDA) receptor (NMDAR) activity regulates the net number of  $\alpha$ -amino-3-hydroxy-5-methyl-4-isoxazolepropionic acid (AMPA) receptors (AMPA) at the cell surface by modulating the balance between AMPAR membrane insertion and endocytosis. In this study, we addressed the role of NMDAR subtypes and of NMDAR-mediated  $\text{Ca}^{2+}$  influx in the NMDAR-induced endocytosis of GluR2-containing AMPARs in primary murine hippocampal neurons. We found that NMDAR activation enhanced the endocytosis of AMPARs containing the GluR2 splice variants with short, but not long, cytoplasmic tails. NMDA-induced GluR2 endocytosis was completely inhibited by pharmacological block of NR2B-containing NMDARs. In turn, preferential block of NR2A-containing

NMDARs did not affect NMDA-induced AMPAR endocytosis, indicating that AMPAR internalization is controlled by a restricted set of NMDARs. The NMDA-induced GluR2 internalization was also observed in the absence of extracellular  $\text{Na}^+$  ions, suggesting that membrane depolarization is not a prerequisite for this effect. Furthermore, the activation of  $\text{Ca}^{2+}$ -impermeable NMDARs containing the mutant NR1(N598R) subunit failed to enhance AMPAR endocytosis, indicating a requirement of  $\text{Ca}^{2+}$  influx directly through the NMDAR channels. In summary, our findings suggest that the NMDAR-induced selective internalization of short C-terminal GluR2-containing AMPARs requires a  $\text{Ca}^{2+}$  signal that originates from NMDAR channels and is processed in an NMDAR subtype-restricted manner.

The regulation of AMPAR membrane density by NMDAR activity is a key mechanism for the expression of NMDAR-dependent plasticity via the membrane insertion or endocytosis of AMPARs (Malenka and Bear, 2004; Kim et al., 2005; Zhu et al., 2005). The early determinants in the NMDAR

signaling leading to AMPAR internalization are largely unknown.

AMPA channels are formed by heterotetrameric combinations of GluR1–4 subunits that determine the electrophysiological properties of AMPARs and govern their trafficking via C-terminal cytoplasmic domains (Sheng and Kim, 2002; Collingridge et al., 2004). The GluR2 subunit is particularly relevant in that it renders AMPAR channels impermeable to  $\text{Ca}^{2+}$  (Dingledine et al., 1999) and is present in the predominant AMPAR heteromers of pyramidal hippocampal neurons (Wenthold et al., 1996). The cytoplasmic tail of the short GluR2 C-terminal splice variant “drives” the constitutive recycling and the NMDAR-induced internalization of AMPARs (Shi et al., 2001; Lee et al., 2004). In contrast, the long GluR2 C-terminal splice variant contributes to

This work was funded by a Wellcome Trust Senior Fellowship and a Wellcome grant to R.S., and a Biotechnology and Biological Sciences Research Council grant to M.S. and R.S. C.M.T. was supported in part by a Wellcome Trust Traveling Fellowship, and G.F.R. was the recipient of a Deutsche Forschungsgemeinschaft Emma Noether Fellowship.

<sup>1</sup> Current affiliation: Department of Psychiatry and Behavioral Sciences, Stanford University, Stanford, CA.

<sup>§</sup> The online version of this article (available at <http://molpharm.aspetjournals.org>) contains supplemental material.

Article, publication date, and citation information can be found at <http://molpharm.aspetjournals.org>.  
doi:10.1124/mol.105.018580.

**ABBREVIATIONS:** AMPAR,  $\alpha$ -amino-3-hydroxy-5-methyl-4-isoxazolepropionic acid receptor; AMPA,  $\alpha$ -amino-3-hydroxy-5-methyl-4-isoxazolepropionic acid; NMDAR, *N*-methyl-D-aspartate receptor; NMDA, *N*-methyl-D-aspartate; LTP, long-term potentiation; LTD, long-term depression; UTR, untranslated region; (E)GFP, (enhanced) green fluorescent protein; DIV, days in vitro; aCSF, artificial cerebrospinal fluid; KA, kainate; IFP, ifenprodil; NVP, NVP-AAM077; NVP-AAM077, the active diastereomer of (1*RS*,1*S*)-PEAQX, which is [(*R*)-[(*S*)-1-(4-bromophenyl)-ethylamino]-(2,3-dioxo-1,2,3,4-tetrahydroquinoxalin-5-yl)-methyl]-phosphonic acid; HS, horse serum; APV, 2-amino-5-phosphonopentanoic acid; Ro, Ro25-6981; Ro25-6981, ( $\pm$ )-(*R*\*,*S*\*)- $\alpha$ -(4-hydroxyphenyl)- $\beta$ -methyl-4-(phenylmethyl)-1-piperidine propanol; TRITC, tetramethylrhodamine isothiocyanate; E-GluR2-S, EGFP-tagged GluR2, short C terminus; E-GluR2-L, EGFP-tagged GluR2, long C terminus; I-V, current-voltage.

AMPA membrane insertion (Kolleker et al., 2003), as do GluR1 and the long C-terminal splice variant of GluR4 (Hayashi et al., 2000; Zhu et al., 2000), or to AMPAR removal during depotentiation (Zhu et al., 2005). The contribution of the long GluR2 C-terminal splice variant to AMPAR endocytosis induced by acute NMDAR activation, however, remains unknown.

NMDAR subtypes are heterotetrameric complexes typically formed by NR1 and NR2A-D subunits (Wenthold et al., 2003). In the hippocampus and the neocortex, NR2B predominates in early postnatal life, whereas NR2A is gradually expressed during the first two postnatal weeks, resulting in diheteromeric (NR1/NR2A, NR1/NR2B) and triheteromeric (NR1/NR2A/NR2B) receptor subtypes (Kew et al., 1998). This developmental profile is paralleled in vitro (Li et al., 2002).

Both NMDAR-dependent synaptic long-term potentiation (LTP) and depression (LTD), and the NMDAR-induced membrane insertion or removal of AMPARs require a postsynaptic  $Ca^{2+}$  transient elicited by NMDAR activation (Lisman, 1989; Sheng and Kim, 2002). Beyond the model in which the  $Ca^{2+}$  signal kinetics directs the balance of this duality (Lisman, 1989), recent observations suggest that the NR2 subunit composition of NMDAR complexes plays a decisive role in the effects downstream of NMDAR activation (Liu et al., 2004; Massey et al., 2004; Kim et al., 2005).

Here, we investigated the role of NMDAR subtypes in the NMDA-induced endocytosis of surface AMPARs containing N-terminally EGFP-tagged GluR2 expressed in hippocampal cultures using a Sindbis virus-derived system. NMDAR activation enhanced the intracellular accumulation of AMPARs containing the short, but not the long C-terminal splice variant of GluR2. This effect was initiated by NR2B- but not NR2A-containing NMDARs and required  $Ca^{2+}$  influx through the activated NMDAR channels. We propose that NR2B-specific processing of the  $Ca^{2+}$  signals carried by NMDARs constitute an early step in the regulated AMPAR endocytosis.

## Materials and Methods

**Materials.** All chemicals and drugs were obtained from Sigma (Poole, Dorset, UK), unless specified otherwise.

**Animal Procedures.** Procedures were performed according to the Animals Scientific Procedures Act of 1986, under license of the Home Office. Animals were kept at the Biological Services Unit of the University College London.

**Sindbis Virus Expression of Recombinant E-GluR2 in Cultured Neurons.** We constructed an N-terminally EGFP-tagged GluR2 subunit following a strategy similar to that described by Shi et al. (1999). A multistep cloning procedure resulted in a construct containing from the 5' to the 3' end: the 5'-UTR from *Xenopus laevis* hemoglobin, rat GluR1 signal peptide, and four amino acid residues beyond the signal-peptide-cleavage site, EGFP coding sequence from vector pEGFP-N1 (Clontech, Mountain View, CA), rat GluR2 flop coding sequence from codon 21 onward, and the Sindbis-specific 3'-UTR and poly(A) tail from the SINrep(nsP2S726) plasmid (Kim et al., 2004). The relevant DNA sequences were confirmed by sequencing and submitted to the European Molecular Biology Laboratory as pGFP-GluR2-Sin (accession number AJ870439). For the generation of short and long C-terminal GluR2 splice variants, the respective sequences were amplified by RT-PCR from total brain mouse E17 RNA, encoding the amino acid residues from Y837KSR (TACAAGT-CAAGGG) onward through a sequence common to both splice variants (CCTTGAATTGTAAG, 130 base pairs beyond the STOP codon

in the 3'-UTR of the long splice variant), and shuttled into pGFP-GluR2-Sin. The splice variant-specific sense primers were 5'-TACAAGTCAAGGGCCGAGGCGAAACGAATGAAGGTGGCAAAGAAT (for GluR2 short) and 5'-TACAAGTCAAGGGCCGAGGCGAAACGAATGAAGATGACCTTGAGC (for GluR2 long). The common antisense primer was 5'-CCTTGAATTGTAAGGAAAGATTACTCGAGG-GCCTACGT.

pGFP-GluR2-Sin constructs with short and long C-terminal splice variants were shuttled into SINrep(nsP2S726) with XbaI and NotI, and recombinant Sindbis replicons were generated as described previously (Kim et al., 2004; Specht et al., 2005). Virions were harvested 24 to 36 h after transfection of  $1 \times 10^7$  BHK-21 cells, typically yielding in the range of  $10^6$  infectious units/ml.

**Primary Mouse Hippocampal Neuron Cultures.** Primary hippocampal cultures were generated from individual animals either at embryonic day 16 for NR1 mutant mice or otherwise at postnatal day 0, as described previously (Specht et al., 2005), and fed weekly by replacing half of the culture medium with a freshly prepared one. Experiments were performed on cultures between days in vitro (DIV) 14 and 21. Cells expressing EGFP-tagged GluR2 were used 18 to 28 h after infection with Sindbis virions. Viral titers were adjusted to yield 20 to 30% green fluorescent cells.

**Electrophysiology.** Cultures at DIV 14 to 21 were placed in a recording chamber and perfused at room temperature (RT, 20–25°C) with artificial CSF (aCSF; 124 mM NaCl, 2.4 mM KCl, 2 mM  $CaCl_2$ , 2 mM  $MgCl_2$ , 1.2 mM  $NaH_2PO_4$ , 26 mM  $NaHCO_3$ , and 20 mM glucose, pH 7.4, saturated with 95%  $O_2$  + 5%  $CO_2$ ), and containing 200 nM tetrodotoxin (Tocris, Northpoint, Avonmouth, UK), 10  $\mu$ M bicuculline methiodide, and 1  $\mu$ M strychnine. Where necessary, infected cells were identified by their green fluorescence.

Rectification of kainate-induced AMPAR responses was determined in whole-cell, voltage-clamp mode by local superfusion of 100  $\mu$ M kainate (KA) in aCSF, either by voltage ramps from  $-70$  to  $50$  mV (0.1 mV/ms) at constant perfusion or by holding at discrete potentials and switching of superfusion. Series resistance was compensated at 80 to 95%. In the case of voltage ramps, leakage current was determined in the absence of agonist and subtracted. Glass pipettes for whole-cell patch recordings (4–6 M $\Omega$  resistance) were filled with 115 mM cesium methanesulfonate, 20 mM CsCl, 10 mM HEPES, 2.5 mM  $MgCl_2$ , 4 mM  $Na_2ATP$ , 0.4 mM  $Na_3GTP$ , 10 mM sodium phosphocreatine, 0.6 mM EGTA, and 0.1 mM spermine, pH 7.25. NMDA-induced responses were obtained in nominally  $Ca^{2+}$ - and  $Mg^{2+}$ -free aCSF, containing 20  $\mu$ M 2,3-dihydroxy-6,7-dinitroquinoxaline, at  $-60$  mV. aCSF containing 20  $\mu$ M NMDA and 10  $\mu$ M glycine was applied by bath perfusion. NMDAR antagonists ifenprodil (IFP, 10  $\mu$ M), or NVP-AAM077 (NVP, 1  $\mu$ M; Novartis Pharma, Basel, Switzerland) were preapplied for 2 min and present during agonist application.

Data were collected using an Axopatch 200B amplifier (Molecular Devices, Sunnyvale, CA), filtered at 5 kHz, digitized and streamed to disk, using CellWorks software (npi electronic, Tamm, Germany). Off-line analysis and graphs were produced using Igor Pro 4 (WaveMetrics, Lake Oswego, OR), or Scilab 3.0 (<http://scilabsoft.inria.fr>).

**Immunofluorescence Protocol for GluR2 Internalization.** To visualize the internalization of AMPARs containing either endogenous or recombinant EGFP-tagged GluR2 we used an antibody-feeding protocol (see Supplementary Table SI for a schematic protocol and duration of live antibody incubations). Antibodies were diluted in equilibrated culture medium containing 5% heat-inactivated horse serum (HS; Invitrogen, Carlsbad, CA). Live antibody incubations were followed by three washes (amounting to 1 min) in the same medium. The surface EGFP-tagged receptors were initially labeled live with unconjugated anti-GFP rabbit antiserum (1:100; Abcam, Cambridge, UK) under normal culture conditions. For the activation of NMDARs, the cultures were washed (1 min) at room temperature in aCSF, then treated for 2 min with agonist as indicated in figure legends. Unstimulated controls consisted of cultures treated only with aCSF. After treatment, the cells were washed

again in aCSF (1 min) and returned to normal culture conditions. Drugs were applied in  $Mg^{2+}$ -free buffers, in the presence of 20  $\mu M$  2,3-dihydroxy-6,7-dinitroquinoxaline, 200 nM tetrodotoxin, 10  $\mu M$  bicuculline methiodide, and 1  $\mu M$  strychnine. When used, NMDAR antagonists (APV, IFP, Ro, or NVP) were preapplied during the aCSF wash, and thus were present throughout the 3-min period (concentrations as indicated in figure legends). For the experiments in Fig. 4A, HEPES-Ringer (126 mM NaCl, 2.4 mM KCl, 2 mM  $CaCl_2$ , 2 mM  $MgCl_2$ , and 5 mM HEPES, pH 7.35) was used instead of aCSF, with sodium chloride substituted with choline chloride for solutions without sodium.

Cultures were then returned to normal conditions for the durations given in figure legends and Table SI, and surface and internalized EGFP-tagged GluR2 on the same cells were stained by successive application of secondary antibodies. To reveal the subpopulation of EGFP-tagged GluR2 still present at the cell surface, cultures were stained live with Cy5-conjugated goat anti-rabbit IgG (15  $\mu g/ml$  in HS-containing culture medium; Jackson ImmunoResearch Laboratories, West Grove, PA). After a brief wash in the same medium, the cultures were fixed [4% paraformaldehyde and 1% sucrose in phosphate buffer (0.1 M  $NaH_2PO_4$ , pH 7.5, 10 min)], permeabilized and blocked with blocking solution (phosphate buffer containing 0.3% Triton X-100 and 5% HS, 30 min). The internalized subpopulation of EGFP-tagged GluR2 was stained with a rhodamine (TRITC)-conjugated anti-rabbit IgG (15  $\mu g/ml$  in blocking solution, 30 min; Jackson ImmunoResearch Laboratories). For the staining of presynaptic terminals, a mouse monoclonal anti-synaptophysin antibody (10  $\mu g/ml$ ; Chemicon, Temecula, CA) was included in this step, and was followed by incubation with 7-amino-4-methylcoumarin-3-acetic acid-conjugated goat anti-mouse IgG (15  $\mu g/ml$ ; Jackson ImmunoResearch Laboratories). Cultures were finally washed in phosphate buffer and mounted in Gel-Mount (Sigma, St. Louis, MO). When specified, nuclei were counterstained with Hoechst 33258 (1  $\mu g/ml$  in phosphate-buffered saline; Invitrogen) for 5 min at room temperature, before mounting.

The specificity of the anti-GFP immunostaining for the surface-targeted EGFP-tagged GluR2 was confirmed by the lack of GFP immunoreactivity in naive cultures (i.e., not infected with EGFP-tagged GluR2 Sindbis virus), as shown in Supplementary Fig. S1. We also confirmed the ability of the Cy5-conjugated antibody to saturate the EGFP-tagged GluR2-anti-GFP immunocomplexes still present at the cell surface by performing a test immunostaining where Cy5- and TRITC-conjugated antibodies were successively applied live, before fixation. Under these circumstances, no signal was detected from the second, TRITC-conjugated antibody (Supplementary Fig. S2).

The internalization of the AMPARs containing native endogenous GluR2 subunit was visualized by a similar protocol, using a monoclonal antibody against the GluR2 N-terminal amino acids 175 to 430 (MAB397, 17  $\mu g/ml$  in HS-containing culture medium; Chemicon) followed by Cy5-conjugated goat anti-mouse IgG (15  $\mu g/ml$  in HS-containing culture medium; Jackson ImmunoResearch) and Cy3-conjugated goat anti-mouse IgG (15  $\mu g/ml$  in HS-containing culture medium; Jackson ImmunoResearch) for surface and internalized GluR2, respectively. The specificity of anti-GluR2 antibody was confirmed by the lack of immunoreactivity on *Gria2*<sup>-/-</sup> neurons (data not shown).

**Confocal Microscopy and Image Analysis.** Multichannel fluorescence confocal images were acquired on a LSM 510 Meta laser scanning confocal microscope (Carl Zeiss GmbH, Jena, Germany) with an oil-immersion Plan-Apochromat objective (63 $\times$ , numerical aperture 1.40). Excitation/emission filter wavelengths were 364 nm/385 nm long-pass for 7-amino-4-methylcoumarin-3-acetic acid and Hoechst 33258, 488 nm/505–550 nm for EGFP, 543 nm/568 nm to 610 nm for TRITC or Cy3 and 633 nm/664 nm to 717 nm for Cy5. Fluorescence channels were acquired in sequential line-scan mode to minimize channel cross talk. Pinholes were set to 1 Airy disk unit and acquisition parameters were adjusted close to full dynamic range, independently for each channel.

Confocal data were acquired blindly with respect to the experimental conditions, from neurons showing clear anti-GluR2 or green fluorescent cells with anti-EGFP immunofluorescent puncta in conventional fluorescence. The acquisition field (146  $\times$  146  $\mu m$ ) was centered on the soma. Optical slices (20–50) were recorded with a resolution of 140 nm (lateral) and 240 nm (axial) and stored as multichannel 16-bit image files.

Image analysis was performed separately on the three-dimensional fluorescence data sets for the Cy5 and TRITC channels using ImageJ software (<http://rsb.info.nih.gov/ij/>). Grayscale fluorescent images were converted to 32-bit floating point and were processed through a median filter to remove photomultiplier noise. To isolate immunofluorescent E-GluR2 puncta from the background, images were segmented using bilevel thresholding based on the gray level histogram. Threshold values were initially determined by the automatic threshold feature of ImageJ, based on an iterative algorithm and then were manually lowered under visual control to encompass all immunofluorescent puncta, which typically meant pixels above 1/10 of the maximum gray value in the image. Similar results were obtained with an automated thresholding algorithm based on gray level histogram entropy. Subsequently, structures 1 pixel wide were removed from the segmented images by one iteration of morphological opening. Images were analyzed blindly with respect to the experimental conditions.

The internalized fraction of GluR2 subunit was expressed quantitatively as the ratio between the count of thresholded voxels in the TRITC (for EGFP-tagged GluR2) or Cy3 (for the endogenous GluR2) channel and the sum of thresholded voxels in TRITC or Cy3 and Cy5 channels. The raw values for the internalized fraction in our experiments are given in the Supplementary Table SI. The data shown in the figures represent mean  $\pm$  S.E.M. of the internalization index obtained by normalizing the internalized fraction to the values obtained in unstimulated cells within each experimental group, as indicated in the legends. The numbers of neurons used in the analysis are indicated in figure legends and in Supplemental Table SI and represent data, typically from three coverslips for each condition. Illustrations show Z-projected fluorescence confocal stacks overlaid in pseudocolor using The GNU Image Manipulation Program (<http://www.gimp.org/>).

## Results

**N-Terminally EGFP-Tagged GluR2 Reconstitutes the GluR2 Phenotype in *Gria2*<sup>-/-</sup> Neurons.** To visualize the subcellular distribution of GluR2-containing AMPARs, we constructed a recombinant N-terminally EGFP-tagged, short C-terminal splice variant GluR2 (E-GluR2-S), and expressed it in primary hippocampal neurons using a Sindbis virus-derived system. E-GluR2-S-expressing neurons exhibited finely grained somatodendritic fluorescence from the EGFP tag within 24 h of infection. To confirm that our expression system delivered subunits that formed functional AMPAR channels, we analyzed the I-V relationship of whole-cell AMPAR currents in GluR2 knockout (*Gria2*<sup>-/-</sup>) neurons infected with virus encoding E-GluR2-S.

Currents elicited with 100  $\mu M$  KA in uninfected wild-type neurons displayed a linear I-V relationship (Fig. 1A). In contrast, whole-cell responses to KA in uninfected *Gria2*<sup>-/-</sup> neurons had the expected inward rectifying I-V relationship (Fig. 1A) characteristic of the GluR2-lacking AMPARs in these animals (Jia et al., 1996). Expression of E-GluR2-S rescued the wild-type AMPAR phenotype in *Gria2*<sup>-/-</sup> neurons. KA responses from *Gria2*<sup>-/-</sup> neurons infected with E-GluR2-S virus had a near-linear I-V relationship (Fig. 1A) with a rectification index of  $0.4 \pm 0.13$  (Fig. 1B), significantly

different from uninfected *Gria2*<sup>-/-</sup> cells ( $0.06 \pm 0.03$ ,  $p < 0.05$ ) and near the values in uninfected wild-type neurons ( $0.72 \pm 0.11$ ).

These results demonstrate that our recombinant subunit was functional and was incorporated into newly synthesized AMPARs targeted at the cell surface. AMPAR subunits have been reported to form homomeric receptors when expressed in vitro (Shi et al., 2001). Homomeric GluR2 receptors typically yield agonist-induced currents 1 order of magnitude smaller than heteromeric GluR1/2 receptors (Keinanen et al., 1990). In our system however, currents elicited by KA in E-GluR2-S-expressing *Gria2*<sup>-/-</sup> neurons were comparable in amplitude to those recorded from wild-type neurons where heteromeric AMPARs are natively predominant ( $-611.14 \pm 166.4$  pA and  $-756 \pm 207.5$  pA, respectively, at  $-60$  mV holding potential). Taken together, this indicates the existence of heteromeric GluR1/E-GluR2-S receptors in infected *Gria2*<sup>-/-</sup> cells, possibly at a relative proportion similar to that of heteromeric GluR1/GluR2 in wild-type neurons.

**NMDAR-Induced E-GluR2-S AMPAR Internalization.** We determined the internalization of E-GluR2-S AMPARs using a live antibody-feeding protocol (see *Materials and Methods*). Under confocal microscopy examination, the anti-GFP-stained cell surface E-GluR2-S appeared as abundant Cy5-fluorescent puncta decorating the soma and the dendritic arborizations, whereas the anti-GFP-stained E-GluR2-S that had been internalized after receptor activation as TRITC-fluorescent puncta located in the soma and dendritic shafts (Fig. 2A). Costaining for the presynaptic marker synaptophysin revealed that most of the cell surface puncta were in the proximity of synaptic terminals (Fig. 5B).

Activation of NMDARs for 2 min with  $20 \mu\text{M}$  NMDA and  $10 \mu\text{M}$  Gly enhanced E-GluR2-S internalization above the constitutive levels of unstimulated cells, as early as 5 min after agonist washout (see Supplementary Fig. S3 and Supplementary Table SI, rows 3–14). Twenty minutes after NMDAR activation, the E-GluR2-S endocytosis was enhanced by  $2.31 \pm 0.32$ -fold and was blocked by  $50 \mu\text{M}$  APV ( $0.93 \pm 0.08$  times unstimulated controls; Fig. 2B and Table SI, row 70). A more intense stimulus ( $100 \mu\text{M}$  NMDA and  $1 \mu\text{M}$  Gly for 2 min) enhanced the E-GluR2-S internalization with a similar time course and was blocked by  $100 \mu\text{M}$  APV (Supplementary Table SI, rows 15–20 and 71).

Strictly speaking, this assay does not measure the amount

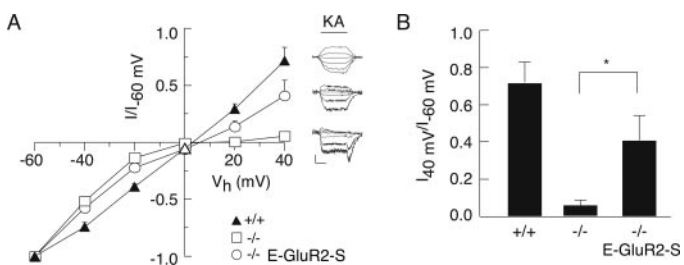


**Fig. 1.** E-GluR2-S rescues wild-type AMPAR phenotype in *Gria2*<sup>-/-</sup> neurons. **A**, left: I-V relationships of  $100 \mu\text{M}$  kainate-evoked whole-cell steady-state currents of cultured hippocampal wild-type neurons (triangles,  $n = 5$  cells), naive *Gria2*<sup>-/-</sup> neurons (squares,  $n = 4$ ) and *Gria2*<sup>-/-</sup> neurons expressing E-GluR2-S (circles,  $n = 4$ ). Right, representative kainate responses for the individual genotypes at holding membrane potential ( $V_h$ ) starting at  $-60$  mV in  $20$ -mV increments. Horizontal bar indicates kainate application (5 s); scale bars,  $100$  pA and  $2$  s. **B**, rectification indices for the recordings shown in **A**. Data are means  $\pm$  S.E.M. of the values normalized to the currents at  $-60$  mV;  $*$ ,  $p < 0.05$ .

of endocytosed receptors per se but instead shows the amount of prelabeled, formerly at the surface receptors that got internalized but not recycled or degraded before fixation. Kinetic studies, however, indicate that the measured signal is a valid representation of the actually internalized fraction, in particular at short incubation periods (Supplementary Fig. S3A and Fig. 5A; Lee et al., 2004). With respect to the regulated endocytosis, in our hands, longer incubation periods consistently provided qualitatively comparable results, although they probably underestimate the actual extent of the regulated endocytosis (see Supplementary Table SI).

To test whether our use of a recombinant expression system tainted our findings, we performed this assay on native, endogenous GluR2 containing AMPARs. Figure 2C shows a

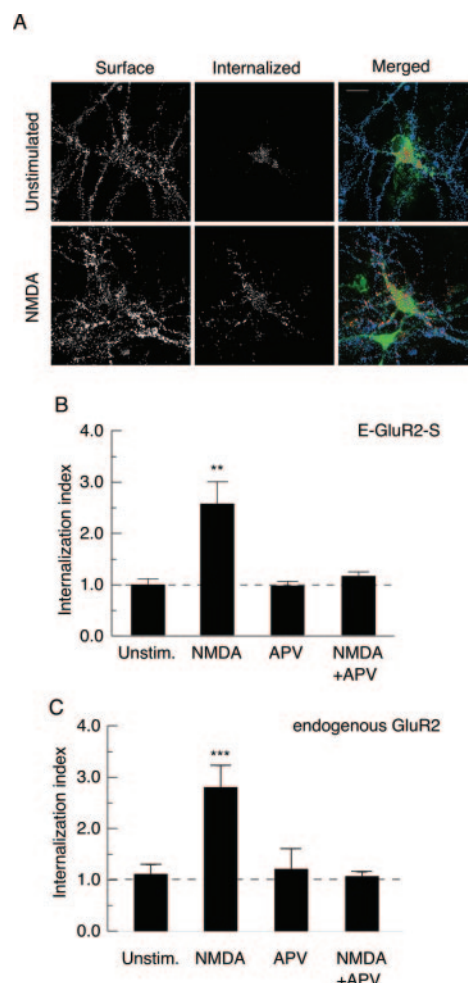


**Fig. 2.** NMDAR-induced internalization of E-GluR2-S-containing AMPARs. **A**, Z-axis-projected confocal images of *Gria2*<sup>-/-</sup> neurons expressing recombinant E-GluR2-S (green in merged) with anti-GFP immunofluorescence for surface (blue in merged) and internalized (red in merged) E-GluR2-S AMPARs 60 min after treatment with aCSF alone (unstimulated) or agonist (NMDA,  $100 \mu\text{M}$  NMDA +  $1 \mu\text{M}$  Gly). Antibody staining as in Supplementary Table SI, rows 33 and 38. Scale bar,  $20 \mu\text{m}$ . **B**, internalization of E-GluR2-S in wild-type neurons 20 min after stimulation with  $20 \mu\text{M}$  NMDA +  $10 \mu\text{M}$  Gly alone (NMDA,  $n = 15$ ) or in the presence of  $50 \mu\text{M}$  APV (NMDA + APV,  $n = 5$ ) or after  $50 \mu\text{M}$  APV only (APV,  $n = 5$ ). The bars represent mean  $\pm$  S.E.M. internalized fraction (10 min live antibody incubations) normalized to unstimulated controls (Unstim.;  $n = 19$ ). Raw data are in Table SI, rows 6 (Unstim.), 12 (NMDA), 68 (APV), and 70 (NMDA + APV). **C**, internalization of native, endogenous GluR2-containing AMPARs in wild-type cells, 5 min after treatment as in **B**; raw data are in Table SI, rows 83 to 86. \*\*,  $p < 0.01$ ; \*\*\*,  $p < 0.001$  compared with unstimulated controls.

NMDAR-dependent endocytosis of GluR2 essentially as we had found for the recombinant subunits and in line with published observations (Lee et al., 2004).

**NR2B- but Not NR2A-Containing NMDARs Control GluR2-AMPA Endocytosis.** NMDAR-induced changes in AMPAR membrane density are likely to reflect the direction of NMDAR-induced synaptic plasticity. We tested here the hypothesis that NR2B subunits may selectively link NMDAR activation with the endocytosis of GluR2-containing AMPARs. Therefore, we used NR2B-selective antagonists, namely IFP (Williams, 1993) and Ro (Fischer et al., 1997), and the NR2A-preferring antagonist NVP (Liu et al., 2004; Weitlauf et al., 2005) to investigate the involvement of the NR2B- and NR2A-containing NMDARs in the control of E-GluR2-S endocytosis.

First, we determined the fractional whole-cell currents elicited by NMDA in the presence of NR2 subtype-selective antagonists. The NR2B-selective antagonist IFP inhibited the NMDA-induced currents by approximately 25%, whereas the NR2A-preferring antagonist NVP reduced currents by approximately 63% (IFP,  $75.3 \pm 5.17\%$ ; NVP,  $36.9 \pm 6.79\%$  of the test responses; Fig. 3A). Although NVP is a potent antagonist for NR2A-containing NMDARs (Auberson et al., 2002; Liu et al., 2004; Massey et al., 2004), its specificity for NR2A and kinetics have been challenged recently (Berberich et al., 2005; Weitlauf et al., 2005). The findings of Berberich et al. (2005) and Weitlauf et al. (2005) confirmed that NVP is an efficient NR2A antagonist under the conditions that we have used (i.e., presence of  $1 \mu\text{M}$  NVP before and during agonist application and when steady-state responses were measured). Under these conditions, NVP also produces a 20 to 30% inhibition of NR2B-containing NMDAR currents.

We have found that NR2B-containing NMDARs carried approximately 25% of the NMDA-induced whole-cell currents. Therefore, approximately five to eight percentage points of the block produced by NVP would represent contaminant NR2B inhibition. The substantially larger block of NMDA-induced currents that we have observed with NVP confirms the existence of NR2A-containing NMDARs in our cultured neurons, in agreement with previously published data (Li et al., 1998).

This demonstrates that both NR2 subunit subtypes are present in our cultures at the stage in vitro when the endocytosis experiments were performed. It is noteworthy that the NR2B-containing NMDAR subtypes carried only the minority of the NMDAR currents.

When we tested the effect of the NR2 subtype-selective antagonists on AMPAR internalization, we observed that both IFP ( $10 \mu\text{M}$ ) and Ro ( $1 \mu\text{M}$ ) blocked the NMDA-induced E-GluR2-S endocytosis (IFP,  $1.03 \pm 0.23$ , and Ro,  $0.8 \pm 0.11$ , compared with unstimulated controls, see Fig. 3, B and C; raw data are given in Table SI, rows 56–65 for IFP and 66–67 for Ro) as efficiently as the unspecific NMDAR antagonist APV. This by itself suggests a special role for NR2B-containing NMDARs in our paradigm. We know from our electrophysiological data that NR2B-containing NMDARs are responsible only for a minority of the NMDA response, whereas the majority is carried by NR2A-containing NMDARs. Therefore, we also tested the effect of NVP, which efficiently blocks the NR2A responses. We observed that NVP ( $1 \mu\text{M}$ ) did not alter the endocytosis of E-GluR2-S

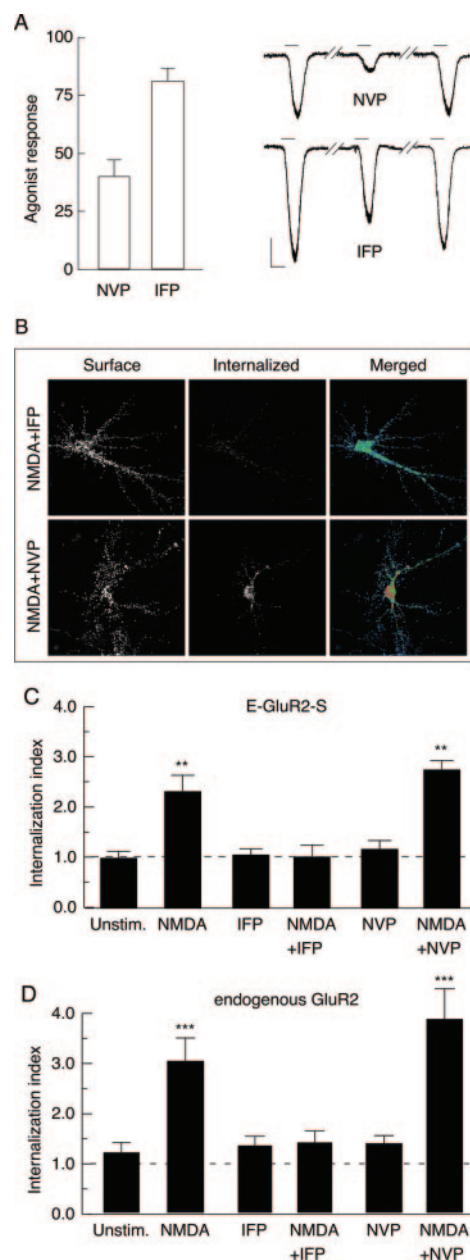


**Fig. 3.** NR2B- but not NR2A-containing NMDARs control the internalization of E-GluR2-S. **A**, left: whole-cell responses to  $20 \mu\text{M}$  NMDA +  $10 \mu\text{M}$  Gly recorded at DIV 15 to 21 in the presence of  $1 \mu\text{M}$  NVP ( $n = 11$ ) or  $10 \mu\text{M}$  IFP ( $n = 9$ ). Right, NMDAR currents in the presence of NVP (top, middle trace) or IFP (bottom, middle trace), shown between consecutive test NMDA responses. Columns represent mean  $\pm$  S.E.M. of steady-state current amplitude normalized to the amplitude of the test response before antagonist perfusion; horizontal bars above traces: agonist application (30 s); scale bars: 100 pA, 30 s. **B**, Z-axis-projected confocal images of E-GluR2-S internalization assay (pseudocolors as in Fig. 2) taken from treatment groups in **C**. Scale bar,  $20 \mu\text{m}$ . **C**, internalization of E-GluR2-S in wild-type cells 20 min after stimulation with  $20 \mu\text{M}$  NMDA +  $10 \mu\text{M}$  Gly (NMDA,  $n = 15$ ) alone or in the presence of either  $10 \mu\text{M}$  IFP (NMDA+IFP,  $n = 8$ ) or  $1 \mu\text{M}$  NVP (NMDA+NVP,  $n = 24$ ). IFP, NVP: cells treated with antagonist only ( $n = 7$  and  $10$ , respectively). Bars represent mean  $\pm$  S.E.M. of internalized fraction normalized to unstimulated controls (Unstim.;  $n = 19$ ). Raw values are in Table SI, rows 6 (Unstim.), 12 (NMDA), 50 (NVP), 56 (IFP), 53 (NMDA+NVP), and 63 (NMDA+IFP). **D**, internalization of the native, endogenous GluR2 AMPARs, determined 5 min after treatment as in **C**; raw data are in Table SI, rows 83 (Unstim.), 84 (NMDA), 87 (IFP), 89 (NMDA+IFP), 90 (NVP), and 91 (NMDA+NVP). \*\*,  $p < 0.01$ , and \*\*\*,  $p < 0.001$  compared with unstimulated controls.

induced by NMDAR activation (Fig. 3, B and C). This effectively rules out NR2A-containing NMDAR as major players in the NMDA-induced GluR2 endocytosis (at least in primary hippocampal neurons). Because we have not found any inhibition of NMDA-induced GluR2 endocytosis with NVP, the reduced NR2 subtype specificity of this compound is not relevant in this context. Neither antagonist significantly affected the constitutive endocytosis of E-GluR2-S (Fig. 3C). These results were reproduced when we used higher agonist concentrations and extended live antibody incubation times (Table SI, rows 51, 55, 57, 65–67, 69, and 71). Our data further suggest that a partial blockage of 20 to 30% of NR2B-containing NMDAR is not sufficient to block NMDA-induced GluR2 endocytosis.

To test the effect of partial block of NR2B-containing NMDARs, we determined the NMDA-induced endocytosis in the presence of concentrations of IFP at and below its  $IC_{50}$  for NR2B (Williams, 1993; Williams et al., 1993). Figure S4 and Table SI, rows 58 to 62, indeed show that, as predicted, such low concentrations of IFP did not inhibit the NMDAR-regulated endocytosis.

Furthermore, experiments on the native endogenous GluR2 receptors revealed the same NR2 subtype dependence (Fig. 3D and Table SI, rows 87–91). Taken together, our findings reveal that the NMDA-induced GluR2 endocytosis is selectively enhanced by NR2B-containing NMDARs.

**NMDARs with  $Ca^{2+}$ -Impermeable Channels Cannot Control AMPAR Endocytosis.** To test for the role of the NMDAR-carried  $Ca^{2+}$  influx in the endocytosis of AMPARs without contributions from the voltage-gated  $Ca^{2+}$  channels, we activated NMDARs in the absence of extracellular  $Na^+$  ions (0 mM  $[Na^+]_o$ ). This protocol allows only  $Ca^{2+}$  ions to enter through the NMDAR channel and reduces the depolarizing effects of the  $Na^+$  ions, which are the main charge carriers of NMDAR currents (Burnashev et al., 1995). Activation of NMDARs under 0 mM  $[Na^+]_o$  effectively increased the internalization of E-GluR2-S comparable with that observed in 126 mM extracellular  $Na^+$  (Fig. 4A and Table SI, rows 75–82).

To further address the role of the  $Ca^{2+}$  influx through the activated NMDAR channels in the regulation of membrane AMPAR removal, we determined the NMDA-induced intracellular accumulation of E-GluR2-S in cultured hippocampal neurons from mice expressing a mutant NMDAR that is impermeable to  $Ca^{2+}$  ions yet is able to undergo agonist-dependent activation (*Grin1*<sup>N598R/-</sup> mice; Rudhard et al., 2003). In *Grin1*<sup>N598R/-</sup> mice, the NMDA-induced whole-cell currents are comparable with those in wild-type littermates. Membrane fraction levels of glutamate receptor subunits, particularly of NR1, NR2A, and NR2B (Rudhard et al., 2003) and the membrane targeting of NMDAR subunits (data not shown), are also similar to those in wild-type littermates, which suggests that the presence of  $Ca^{2+}$ -impermeable NMDARs does not have a global effect on the overall receptor complement.

NMDAR activation in *Grin1*<sup>N598R/-</sup> neurons failed to enhance the E-GluR2-S endocytosis ( $1.09 \pm 0.16$  normalized to unstimulated *Grin1*<sup>N598R/-</sup> neurons, Fig. 4B and Table SI, rows 72 and 73). This observation is in line with the experiments with wild-type neurons in 0 mM  $[Na^+]_o$  and indicates that the fractional  $Ca^{2+}$  currents carried by the NMDAR channels are necessary and sufficient to induce E-GluR2-S

endocytosis. The absolute level of constitutive (i.e., unstimulated) E-GluR2-S internalization determined at 60 min after anti-GFP labeling in *Grin1*<sup>N598R/-</sup> neurons was  $0.4 \pm 0.06$  ( $1.92 \pm 0.3$  times the unstimulated endocytosis in wild-type neurons; Table SI, rows 8 and 72). We observed a comparably high level of unstimulated E-GluR2-S endocytosis in neurons from NR1 knockout mice as well (internalized fraction,  $0.5 \pm 0.05$ ,  $n = 21$ ,  $p < 0.001$  compared with unstimulated wild-type cells; Table SI, row 74). Given the importance of NMDARs in the tonic regulation of AMPAR trafficking (Zhu et al., 2005), it would be expected that the long-term functional loss generated by the lack of NMDAR-carried  $Ca^{2+}$  influx, common to both *Grin1*<sup>N598R/-</sup> and NR1 knockout genotypes, may have altered the tonic levels of AMPAR internalization and turnover.

Taken together, these results indicate that NMDAR-induced enhancement of GluR2-AMPA endocytosis requires a  $Ca^{2+}$  influx directly through the NMDAR channel, despite it representing a minor fraction of the NMDAR current. Considering the earlier observations by Beattie et al. (2000), it seems that in this paradigm, other sources of postsynaptic

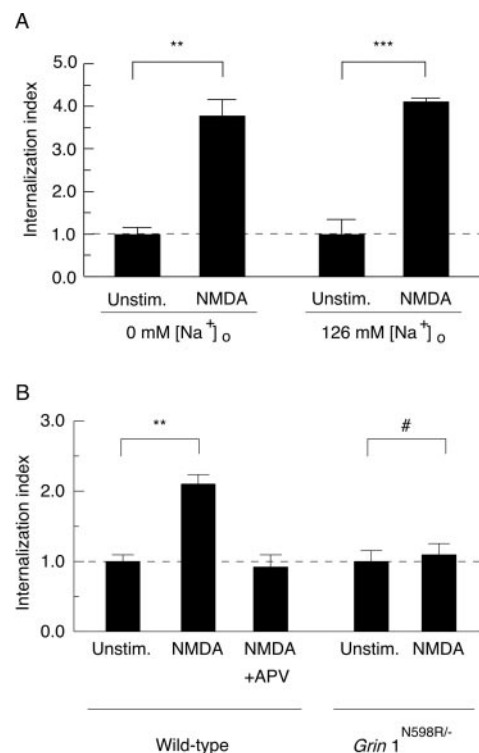


**Fig. 4.** NMDAR-controlled internalization of E-GluR2-S requires  $Ca^{2+}$  influx through NMDAR channels. **A**, E-GluR2-S internalization in wild-type neurons in the absence of extracellular  $Na^+$  (0 mM  $[Na^+]_o$ ) at 5 min under baseline conditions (Unstim.;  $n = 10$ ) and after stimulation with 20  $\mu$ M NMDA + 10  $\mu$ M Gly (NMDA;  $n = 6$ ) or in normal HEPES-Ringer (126 mM  $[Na^+]_o$ ; Unstim.,  $n = 9$ ; NMDA,  $n = 7$ ). Raw data are in Table SI, rows 75, 77, 79, and 81, respectively. **B**, internalization of E-GluR2-S AMPARs in neurons from the indicated genotypes, under baseline conditions (Unstim., wild-type,  $n = 52$ , Table SI, row 8; *Grin1*<sup>N598R/-</sup>,  $n = 12$ , Table SI, row 72) and after NMDAR activation alone (NMDA, wild-type,  $n = 46$ , Table SI, row 20; *Grin1*<sup>N598R/-</sup>,  $n = 15$ , Table SI, row 73) or in the presence of 100  $\mu$ M APV (NMDA + APV,  $n = 24$ , Table SI, row 71). In **B**, internalization was determined with live antibody incubations of 40 min (anti-GFP) and 30 min (Cy5 conjugate), 60 min after treatment. Values are mean  $\pm$  S.E.M. internalized fraction normalized to unstimulated controls within each group. \*,  $p < 0.05$ ; \*\*,  $p < 0.01$ ; \*\*\*,  $p < 0.001$ ; and #,  $p = 0.17$  between data under the brackets.

Ca<sup>2+</sup> rise activated secondary to membrane depolarization cannot substitute for the NMDAR-generated Ca<sup>2+</sup> signal.

**NMDAR Activation Enhances the Intracellular Accumulation of Short but Not Long C-Terminal Splice Variant of E-GluR2.** The interaction domains on the cytoplasmic domains of GluR2 have been studied previously through structure-function analysis (Collingridge et al., 2004). To address the functional role of the native cytoplasmic domain of the GluR2 C-terminal splice variants in the NMDAR-induced removal from the membrane, we expressed E-GluR2-S or EGFP-tagged long C-terminal splice variant (E-GluR2-L) in *Gria2*<sup>-/-</sup> mice.

In contrast to the E-GluR2-S splice variant, NMDA did not enhance the endocytosis of the E-GluR2-L in *Gria2*<sup>-/-</sup> neurons at any time point studied (Fig. 5A and Table SI, rows 29–48). The same GluR2 splice variant dependence was observed on cultures from wild-type *Gria2*<sup>+/+</sup> mice (Fig. 5C and Table SI, rows 3–14 and 21–28). This indicates that in our paradigm, only the short but not the long C-terminal splice variant is subject to NMDAR-controlled endocytosis, which holds true in regardless of the presence of endogenous GluR2 subunits.

## Discussion

The NMDAR-dependent modulation of AMPAR membrane trafficking is an important molecular mechanism in forms of synaptic plasticity where NMDAR activation results in changes of AMPAR membrane density that parallel the changes in synaptic strength (Malenka and Bear, 2004).

To investigate the NMDAR-dependent endocytosis of AMPARs, we expressed N-terminally EGFP-tagged GluR2 subunits (short C-terminal splice variant, E-GluR2-S) in primary hippocampal neurons and determined the NMDA-induced internalization of E-GluR2-S-containing AMPARs with an immunofluorescence-based assay. Although overexpressed individual GluR subunits tend to form homomeric receptors (Shi et al., 2001), our electrophysiological data indicate that E-GluR2-S was incorporated in heteromeric GluR1/E-GluR2-S receptors when expressed in GluR2 knock out background. Furthermore, we observed little difference between the NMDA-induced E-GluR2-S internalization in *Gria2*<sup>-/-</sup> and wild-type neurons (see Table SI and Figure S3A), suggesting that the GluR2 subunit is functionally dominant in the NMDAR-regulated endocytosis of AMPARs, in line with the observations of Lee et al. (2004).

**NMDAR-Controlled Internalization of GluR2 C-Terminal Splice Variants.** The GluR2 subunit exists in two C-terminal splice variants, whose expression levels are developmentally regulated. The long C-terminal splice variant (GluR2-L) is mostly expressed during the first 2 postnatal weeks before being overtaken by the short variant and it contributes to the activity-dependent tonic regulation of synaptic AMPARs trafficking (Kolleker et al., 2003; Zhu et al., 2005). The cytoplasmic domain of GluR2-L is homologous to those of GluR1 and GluR4 (Kohler et al., 1994) and lacks the interaction domains of the short GluR2 C terminus that are involved in NMDAR-dependent internalization of AMPARs (Collingridge et al., 2004). To address the functional role of the long C-terminal GluR2 splice variant in the NMDAR-regulated AMPAR internalization we expressed a recombi-

nant EGFP-tagged long C-terminal splice variant of GluR2 (E-GluR2-L) in *Gria2*<sup>-/-</sup> neurons.

We found that NMDAR activation failed to enhance the internalization of E-GluR2-L in *Gria2*<sup>-/-</sup> neurons, whereas the constitutive level of E-GluR2-L internalization was lower compared with that of the short variant of GluR2. Our observations, together with those of Kolleker et al. (2003), indicate that the developmental transition from GluR2-L expression to the short C-terminal splice variant of GluR2 may substantially affect the NMDAR-dependent targeting and recycling of synaptic AMPARs in hippocampal pyramidal cells in vivo.

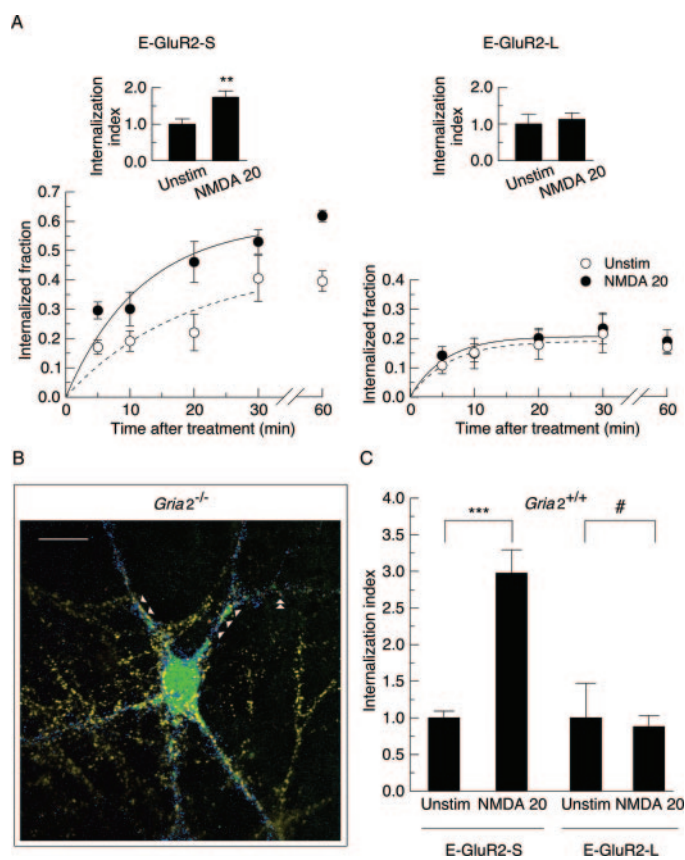


**Fig. 5.** NMDAR-induced internalization of E-GluR2-S-containing AMPARs is restricted to the short splice variant. **A**, internalization of E-GluR2-S and E-GluR2-L in *Gria2*<sup>-/-</sup> neurons, plotted against the time lapsed between stimulation with 20  $\mu$ M NMDA + 10  $\mu$ M Gly (NMDA 20) or under baseline conditions (Unstim); raw data are in Table SI, rows 29–48. Insets, relative internalization at 5 min after stimulation with 20  $\mu$ M NMDA + 10  $\mu$ M Gly (NMDA 20, E-GluR2-S,  $n = 8$ , Table SI, row 34, E-GluR2-L,  $n = 5$ , Table SI, row 44); data are mean  $\pm$  S.E.M. internalized fraction normalized to the unstimulated control (Unstim, E-GluR2-S,  $n = 10$ , Table SI, row 29; E-GluR2-L,  $n = 6$ , Table SI, row 39). Data for time points 5 to 30 min were fitted to one-phase exponential association equation, and correlation coefficients were 0.89 (E-GluR2-S Unstim), 0.93 (E-GluR2-S NMDA 20), 0.90 (E-GluR2-L Unstim) and 0.82 (E-GluR2-L NMDA 20). Data for time point 60 were obtained with antibody incubation times of 40 min (anti-GFP) and 30 min for the Cy5 conjugate. \*\*,  $p < 0.01$ . **B**, E-GluR2-S-expressing *Gria2*<sup>-/-</sup> neuron (green) that has been stained for surface (blue) and internalized (red) E-GluR2-S at 5 min under baseline conditions, and for synaptophysin (yellow). Typical regions of close proximity between surface E-GluR2-S and synaptophysin-positive structures are indicated by arrowheads; the double arrowhead indicates an area where E-GluR2-S internalization has occurred; scale bar, 20  $\mu$ m. **C**, internalization of E-GluR2-S and E-GluR2-L in wild-type neurons under conditions identical to insets in **A**; raw data are in Table SI, rows 3, 9, 21, and p25, respectively; \*\*,  $p < 0.01$ ; #,  $p = 0.22$  between data under the brackets.

**Specific Role of NR2B-Containing NMDAR Subtypes in GluR2 Endocytosis.** In our paradigm, activation of NMDAR signaling independent of the NMDAR subtype resulted in an increased internalization of GluR2 AMPARs in vitro, in agreement with previous observations (Lee et al., 2004).

We hypothesized that under our experimental conditions, activation of NR2B-containing NMDAR subtypes triggers selective signaling that leads to the endocytosis of GluR2-containing AMPARs. We tested this hypothesis by means of a pharmacological block directed at the NR2 subunit subtypes. For a discussion on the selectivity of the NR2 subtype antagonists that we used, see *Results*.

Selective inhibition of NR2B-containing NMDARs blocked the NMDA-induced intracellular accumulation of E-GluR2-S, whereas the preferential inhibition of NR2A-containing NMDARs had no effect, in line with our hypothesis. Our findings therefore provide direct evidence for a NR2B subtype-specific link between the activation of NMDARs and the downstream signaling leading to GluR2-AMPA endocytosis.

NR2A and NR2B subunits are widely expressed in the central nervous system and are considered the major NR2 subunits in the hippocampus, where their expression is developmentally regulated (Monyer et al., 1994; Kew et al., 1998). At the developmental stage of our cultures, hippocampal neurons express a heterogeneous population of NMDARs, largely formed by NR1/NR2A, NR1/NR2B, and NR1/NR2A/NR2B subtypes, paralleling the developmental profile in vivo (Luo et al., 1997; Kew et al., 1998; Li et al., 2002). NR2B-containing NMDAR subtypes are both extrasynaptic (largely NR1/NR2B) and synaptic, where they contribute to the heterogeneous population of NR1/NR2A and NR1/NR2B diheteromers, along with triheteromeric NR1/NR2A/NR2B (Tovar and Westbrook, 1999; Li et al., 2002; Massey et al., 2004). In our cultures, we found that the whole-cell NMDAR current is carried mainly by NR1/NR2A subtypes, and to a lesser extent by NR2B-containing receptors. At the concentration used in our experiments (10  $\mu$ M), ifenprodil is thought to inhibit both NR1/NR2B and NR1/NR2A/NR2B heteromers (Kew et al., 1998), but not NR1/NR2A diheteromers (Williams, 1993). In lack of a selective antagonist for triheteromeric NMDARs, it is tempting to speculate that the mere presence of NR2B subunits in the NMDAR complex, regardless of the coassembly with NR2A, or of a synaptic versus extrasynaptic location, is sufficient to drive the NMDAR signaling toward the internalization of GluR2-containing AMPARs.

As suggested by the findings of Liu et al. (2004) and of Massey et al. (2004), NR2B-containing NMDARs play a special role in the down-modulation of the synaptic strength. The activation of NMDARs achieved in our experimental paradigm is on a time scale larger than what is usually obtained by electrically induced synaptic activity (e.g., low frequency stimulation protocols). Considering this, our findings are likely to reflect an NR2B-selective contribution to mechanisms of global modulation of synaptic strength alike to synaptic scaling (Turrigiano and Nelson, 2004), or to a more local, Hebbian-type modulation, such as LTD.

**The Role of  $\text{Ca}^{2+}$  Influx Carried by NMDAR Channels in the Regulated Endocytosis of AMPARs.** Similar to NMDAR-dependent LTD, a transient increase of the postsynaptic  $\text{Ca}^{2+}$  concentration after glutamate receptor

activation is required for the regulated internalization of AMPARs and operates at multiple levels, including the clathrin-mediated endocytosis (Collingridge et al., 2004). However, the exact role of the  $\text{Ca}^{2+}$  influx carried by the NMDAR channels in the signaling pathway leading to AMPAR endocytosis is still elusive.

We observed that the removal of extracellular  $\text{Na}^+$  does not alter the capability of activated NMDARs to enhance E-GluR2-S internalization, which suggests that depolarization-dependent  $\text{Ca}^{2+}$  sources are not essential for this effect, in line with earlier observations (Beattie et al., 2000). Furthermore, activation of  $\text{Ca}^{2+}$ -impermeable NMDARs in *Grin1*<sup>N598R/-</sup> mice failed to enhance the intracellular accumulation of E-GluR2-S. Together, these results provide direct evidence that  $\text{Ca}^{2+}$  influx through the activated NMDAR channels (and not from other sources) mediates the NMDAR-dependent signaling cascade for the induction of GluR2 AMPAR endocytosis.

A very likely explanation of our finding is that a  $\text{Ca}^{2+}$  signal localized at the NMDAR-associated complex is the initiating signaling step in this regulated GluR2 AMPARs internalization. Such  $\text{Ca}^{2+}$  nanodomain signals (reviewed in Augustine et al., 2003) rely on  $\text{Ca}^{2+}$  “sensors” located near the  $\text{Ca}^{2+}$  source. The morphological and biochemical correlate of such nanodomains could well be the NMDAR-associated complex as defined by proteomic analysis (Husi et al., 2000).

In conclusion, we have shown that the NMDAR-regulated removal of membrane AMPARs containing the short C-terminal splice variant of GluR2 specifically involves NR2B-containing NMDAR subtypes and relies critically on the  $\text{Ca}^{2+}$  influx carried through NMDARs (Fig. 6). Recent obser-

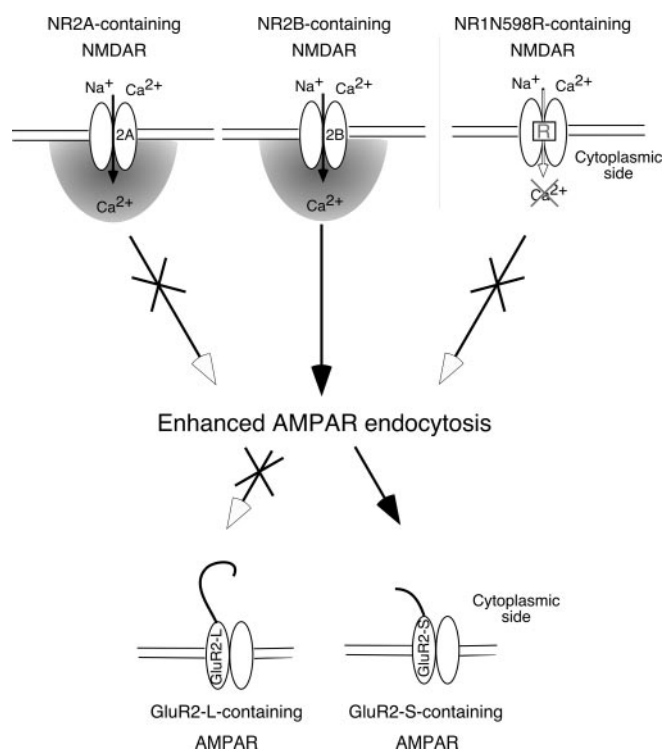


**Fig. 6.** Scheme of the relation between NMDAR (NR2) subtypes, NMDAR-carried  $\text{Ca}^{2+}$  influx and internalization of GluR2-containing AMPAR.  $\text{Ca}^{2+}$  permeation through activated NR2B-containing but not NR2A-containing NMDARs is necessary for the NMDAR-dependent endocytosis of AMPARs that incorporate the short, but not long, C-terminal splice variant of GluR2.



vations by Kim et al. (2005) and Zhu et al. (2005) support the model that different NMDAR subtypes employ different signaling pathways for the modulation of AMPAR trafficking. Our findings suggest that the link between the subunit composition of NMDARs and the selective activation of these pathways may be provided by the highly localized, NR2 subtype-specific processing of the NMDAR-carried  $\text{Ca}^{2+}$  signal.

#### Acknowledgments

We thank Drs. P. Osten and S. Schlesinger for Sindbis vectors.

#### References

- Auberson YP, Allgeier H, Bischoff S, Lingenhoehl K, Moretti R, and Schmutz M (2002) 5-Phosphonomethylquinolinediones as competitive NMDA receptor antagonists with a preference for the human 1A/2A, rather than 1A/2B receptor composition. *Bioorg Med Chem Lett* **12**:1099–1102.
- Augustine GJ, Santamaria F, and Tanaka K (2003) Local calcium signaling in neurons. *Neuron* **40**:331–346.
- Beattie EC, Carroll RC, Yu X, Morishita W, Yasuda H, von Zastrow M, and Malenka RC (2000) Regulation of AMPA receptor endocytosis by a signaling mechanism shared with LTD. *Nat Neurosci* **3**:1291–1300.
- Berberich S, Punnakkal P, Jensen V, Pawlak V, Seeburg PH, Hvalby O, and Kohr G (2005) Lack of NMDA receptor subtype selectivity for hippocampal long-term potentiation. *J Neurosci* **25**:6907–6910.
- Burnashev N, Zhou Z, Neher E, and Sakmann B (1995) Fractional calcium currents through recombinant GluR channels of the NMDA, AMPA and kainate receptor subtypes. *J Physiol* **485** (Pt 2):403–418.
- Collingridge GL, Isaac JT, and Wang YT (2004) Receptor trafficking and synaptic plasticity. *Nat Rev Neurosci* **5**:952–962.
- Dingledine R, Borges K, Bowie D, and Traynelis SF (1999) The glutamate receptor ion channels. *Pharmacol Rev* **51**:7–61.
- Fischer G, Mutel V, Trube G, Malherbe P, Kew JN, Mohacsi E, Heitz MP, and Kemp JA (1997) Ro 25-6981, a highly potent and selective blocker of *N*-methyl-D-aspartate receptors containing the NR2B subunit. Characterization in vitro. *J Pharmacol Exp Ther* **283**:1285–1292.
- Hayashi Y, Shi SH, Esteban JA, Piccini A, Poncer JC, and Malinow R (2000) Driving AMPA receptors into synapses by LTP and CaMKII: requirement for GluR1 and PDZ domain interaction. *Science (Wash DC)* **287**:2262–2267.
- Husi H, Ward MA, Choudhary JS, Blackstock WP, and Grant SG (2000) Proteomic analysis of NMDA receptor-adhesion protein signaling complexes. *Nat Neurosci* **3**:661–669.
- Jia Z, Agopyan N, Miu P, Xiong Z, Henderson J, Gerlai R, Taverna FA, Velumian A, MacDonald J, Carlen P, et al. (1996) Enhanced LTP in mice deficient in the AMPA receptor GluR2. *Neuron* **17**:945–956.
- Keinänen K, Wisden W, Sommer B, Werner P, Herb A, Verdoorn TA, Sakmann B, and Seeburg PH (1990) A family of AMPA-selective glutamate receptors. *Science (Wash DC)* **249**:556–560.
- Kew JN, Richards JG, Mutel V, and Kemp JA (1998) Developmental changes in NMDA receptor glycine affinity and ifenprodil sensitivity reveal three distinct populations of NMDA receptors in individual rat cortical neurons. *J Neurosci* **18**:1935–1943.
- Kim J, Dittgen T, Nimmerjahn A, Waters J, Pawlak V, Helmchen F, Schlesinger S, Seeburg PH, and Osten P (2004) Sindbis vector SINrep(nsP2S726): a tool for rapid heterologous expression with attenuated cytotoxicity in neurons. *J Neurosci Methods* **133**:81–90.
- Kim MJ, Dunah AW, Wang YT, and Sheng M (2005) differential roles of NR2A- and NR2B-containing NMDA receptors in Ras-ERK signaling and AMPA receptor trafficking. *Neuron* **46**:745–760.
- Kohler M, Kornau HC, and Seeburg PH (1994) The organization of the gene for the functionally dominant  $\alpha$ -amino-3-hydroxy-5-methylisoxazole-4-propionic acid receptor subunit GluR-B. *J Biol Chem* **269**:17367–17370.
- Kolleker A, Zhu JJ, Schupp BJ, Qin Y, Mack V, Borchardt T, Kohr G, Malinow R, Seeburg PH, and Osten P (2003) Glutamatergic plasticity by synaptic delivery of GluR-B(long)-containing AMPA receptors. *Neuron* **40**:1199–1212.
- Lee SH, Simonetta A, and Sheng M (2004) Subunit rules governing the sorting of internalized AMPA receptors in hippocampal neurons. *Neuron* **43**:221–236.
- Li B, Chen N, Luo T, Otsu Y, Murphy TH, and Raymond LA (2002) Differential regulation of synaptic and extra-synaptic NMDA receptors. *Nat Neurosci* **5**:833–834.
- Li JH, Wang YH, Wolfe BB, Krueger KE, Corsi L, Stocca G, and Vicini S (1998) Developmental changes in localization of NMDA receptor subunits in primary cultures of cortical neurons. *Eur J Neurosci* **10**:1704–1715.
- Lisman J (1989) A mechanism for the Hebb and the anti-Hebb processes underlying learning and memory. *Proc Natl Acad Sci USA* **86**:9574–9578.
- Liu L, Wong TP, Pozza MF, Lingenhoehl K, Wang Y, Sheng M, Auberson YP, and Wang YT (2004) Role of NMDA receptor subtypes in governing the direction of hippocampal synaptic plasticity. *Science (Wash DC)* **304**:1021–1024.
- Luo J, Wang Y, Yasuda RP, Dunah AW, and Wolfe BB (1997) The majority of *N*-methyl-D-aspartate receptor complexes in adult rat cerebral cortex contain at least three different subunits (NR1/NR2A/NR2B). *Mol Pharmacol* **51**:79–86.
- Malenka RC and Bear MF (2004) LTP and LTD: an embarrassment of riches. *Neuron* **44**:5–21.
- Massey PV, Johnson BE, Moulton PR, Auberson YP, Brown MW, Molnar E, Collingridge GL, and Bashir ZI (2004) Differential roles of NR2A and NR2B-containing NMDA receptors in cortical long-term potentiation and long-term depression. *J Neurosci* **24**:7821–7828.
- Monyer H, Burnashev N, Laurie DJ, Sakmann B, and Seeburg PH (1994) Developmental and regional expression in the rat brain and functional properties of four NMDA receptors. *Neuron* **12**:529–540.
- Rudhard Y, Kneussel M, Nassar MA, Rast GF, Annala AJ, Chen PE, Tigaret CM, Dean I, Roes J, Gibb AJ, et al. (2003) Absence of Whisker-related pattern formation in mice with NMDA receptors lacking coincidence detection properties and calcium signaling. *J Neurosci* **23**:2323–2332.
- Sheng M and Kim MJ (2002) Postsynaptic signaling and plasticity mechanisms. *Science (Wash DC)* **298**:776–780.
- Shi S, Hayashi Y, Esteban JA, and Malinow R (2001) Subunit-specific rules governing AMPA receptor trafficking to synapses in hippocampal pyramidal neurons. *Cell* **105**:331–343.
- Shi SH, Hayashi Y, Petralia RS, Zaman SH, Wenthold RJ, Svoboda K, and Malinow R (1999) Rapid spine delivery and redistribution of AMPA receptors after synaptic NMDA receptor activation. *Science (Wash DC)* **284**:1811–1816.
- Specht CG, Tigaret CM, Rast GF, Thalhammer A, Rudhard Y, and Schoepfer R (2005) Subcellular localisation of recombinant  $\alpha$ - and  $\gamma$ -synuclein. *Mol Cell Neurosci* **28**:326–334.
- Tovar KR and Westbrook GL (1999) The incorporation of NMDA receptors with a distinct subunit composition at nascent hippocampal synapses in vitro. *J Neurosci* **19**:4180–4188.
- Turrigiano GG and Nelson SB (2004) Homeostatic plasticity in the developing nervous system. *Nat Rev Neurosci* **5**:97–107.
- Weitlauf C, Honse Y, Auberson YP, Mishina M, Lovinger DM, and Winder DG (2005) Activation of NR2A-containing NMDA receptors is not obligatory for NMDA receptor-dependent long-term potentiation. *J Neurosci* **25**:8386–8390.
- Wenthold RJ, Petralia RS, Blahos J 2nd, and Niedzielski AS (1996) Evidence for multiple AMPA receptor complexes in hippocampal CA1/CA2 neurons. *J Neurosci* **16**:1982–1989.
- Wenthold RJ, Prybylowski K, Standley S, Sans N, and Petralia RS (2003) Trafficking of NMDA receptors. *Annu Rev Pharmacol Toxicol* **43**:335–358.
- Williams K (1993) Ifenprodil discriminates subtypes of the *N*-methyl-D-aspartate receptor: selectivity and mechanisms at recombinant heteromeric receptors. *Mol Pharmacol* **44**:851–859.
- Williams K, Russell SL, Shen YM, and Molinoff PB (1993) Developmental switch in the expression of NMDA receptors occurs in vivo and in vitro. *Neuron* **10**:267–278.
- Zhu JJ, Esteban JA, Hayashi Y, and Malinow R (2000) Postnatal synaptic potentiation: delivery of GluR4-containing AMPA receptors by spontaneous activity. *Nat Neurosci* **3**:1098–1106.
- Zhu Y, Pak D, Qin Y, McCormack SG, Kim MJ, Baumgart JP, Velamoor V, Auberson YP, Osten P, van Aelst L, et al. (2005) Rap2-JNK removes synaptic AMPA receptors during depotentiation. *Neuron* **46**:905–916.

**Address correspondence to:** Ralf Schoepfer, Laboratory for Molecular Pharmacology, Department of Pharmacology, UCL, Gower Street, London WC1E 6BT, UK. E-mail: r.schoepfer@ucl.ac.uk